Chapter 1

Spin Amplification

The standard approach to implementing a quantum technology is to identify a physical system that can represent a qubit: it must exhibit two (or more) stable states, it should be manipulable through external fields and possess a long decoherence time. Provided that the system can controllably interact with other such systems, then it may be a strong candidate. Electron and nuclear spins, within suitable molecules or solid state structures, can meet these requirements. However the drawback with spin qubits is that they have not been directly measured through a detection of the magnetic field they produce. The magnetic moment of a single electron spin is orders of magnitude too weak to be detected by standard ESR techniques and even the most sensitive magnetometers still fall short of single spin measurement [1] - meanwhile the situation with nuclear spins is worse still. In a few special systems it is possible to convert the spin information into another degree of freedom. For example, a spin-dependent optical transition allow spin to photon conversion in some crystal defects [2, 3, 4], self-assembled semiconductor quantum dots [5, 6], and trapped atoms held in a vacuum [7]. Alternatively, spin to charge conversion is an established technology in lithographic quantum dots [8]. However, the majority of otherwise promising spin systems do not have such a convenient property [9] and

therefore cannot be measured directly.

One suggested solution is to 'amplify' a single spin, by using a set of ancillary spins that are (ideally) initialised to $|0\rangle$. We would look for a transformation of the form

$$|0\rangle |0\rangle^{\otimes n} \to |0\rangle |0\rangle^{\otimes n} \qquad |1\rangle |0\rangle^{\otimes n} \to |1\rangle |1\rangle^{\otimes n}, \qquad (1.1)$$

the idea being that the n ancillary spins constitute a large enough set that state of the art magnetic field sensing technologies can detect them. Note that the transformation need not be unitary or indeed even coherent: since the intention is to make a measurement of the primary spin, it is not necessary to preserve any superposition (that is, we need not limit ourselves to transformations that take $\alpha |0\rangle |0\rangle^{\otimes n} + \beta |1\rangle |0\rangle^{\otimes n}$ to a cat state like $\alpha |0\rangle^{\otimes n+1} + \beta |1\rangle^{\otimes n+1}$).

This is a rather broadly defined transformation and there are a number of ways that one might perform it. Clearly one would like to find the method that is the least demanding experimentally. Previous authors have proposed schemes using a strictly one-dimensional (1D) homogeneous lattice with continuous global driving [10], and an inhomogeneous three-dimensional (3D) lattice with alternating timed EM pulses [11]. The former result has the advantage of simplicity but the rate at which amplification occurs will inevitably be limited by the single dimension of the array; moreover such a system must be highly vulnerable to imperfect initialisation (i.e. finite temperature).

In this chapter we ~~generalise to~~ a homogeneous two-dimensional (2D) square lattice, showing that a continuous global EM field can drive an amplification process that succeeds at finite temperatures (imperfect initialisation of the ancilla spins) and in the presence of decoherence. By bringing the global EM field onto resonance with certain transitions, we are able to create a set of rules that govern locally how spins propagate over the lattice. We then look at the rate of increase in the total number

of flipped spins as a measure of quality of the scheme. While our focus is on the 2D case, we are also able to predict the performance of the amplification protocol for a homogeneous 3D lattice with continuous driving.

1.1   Reviewing of 1D Model

The case of a 1D lattice has been studied in detail by Lee and Khitrin [10]. Before moving to the 2D spin lattice that will form the core of the chapter, we first recall how to simplify the description of this (semi-infinite) 1D spin chain, with nearest neighbour Ising (ZZ) interactions. Under a microwave driving field of frequency ω, the Hamiltonian is given by

$$\mathcal{H} = \sum_{i=1}^{\infty} \epsilon_i \sigma_z^i + J_i \sigma_z^i \sigma_z^{i+1} + 2\Omega_i \sigma_x^i \cos(\omega t) \tag{1.2}$$

ϵ_i is the on-site Zeeman energy of spin i, and J_i is the magnitude of the coupling between spins i and $i+1$. Ω_i describes the coupling of spin i and the microwave field. In this case, spin $i = 1$ is the one whose state is supposed to be amplified. If we assume that the chain is uniform, such that $\Omega_i = \Omega$, $\epsilon_i = \epsilon$ and $J_i = J$, then moving into a frame rotating at frequency ω, making a rotating wave approximation and setting $\omega = \epsilon$ leads to

$$\mathcal{H} = \sum_{i=1}^{\infty} J\sigma_z^i \sigma_z^{i+1} + \Omega \sigma_x^i. \tag{1.3}$$

In order to understand the dynamics of the system, is it instructive to explicitly separate all terms that involve a particular spin k:

$$\mathcal{H} = J(\sigma_z^{k-1} + \sigma_z^{k+1})\sigma_z^k + \Omega \sigma_x^k + \sum_{i \neq \{k, k-1\}} \Omega \sigma_x^i + J\sigma_z^i \sigma_z^{i+1} + \Omega \sigma_x^{k-1} \tag{1.4}$$

Choosing a driving field such that $\Omega \ll J$ means that spin k will only undergo resonant oscillations when the first term in Eq. 1.4 goes to zero - i.e. when the two spins neighbouring spin k are oriented in opposite directions. In any other configuration the Ising coupling takes the spin k off resonance with the microwave and no appreciable dynamics are expected.

Let us now define a subset of states S that exist in the spin chain Hilbert space, $|n\rangle$, which have the first n spins of the chain in state $|\uparrow\rangle$ with the rest $|\downarrow\rangle$. If the rule we just derived holds exactly these states define a closed subspace. We may then write a very simple isolated Hamiltonian for this subspace:

$$\mathcal{H}_S = \Omega \sum_{n=1}^{\infty} |n\rangle \langle n+1| + |n+1\rangle \langle n|. \tag{1.5}$$

1.2   Extension to 2D Model

With this simplification of the 1D Hamiltonian in mind, we progress now to a semi-infinite square spin lattice with nearest-neighbour ZZ interactions. For this case we have

$$\mathcal{H} = \sum_{i=1}^{\infty} \sum_{j=1}^{\infty} \epsilon \sigma_z^{i,j} + J\sigma_z^{i,j}\sigma_z^{i+1,j} + J\sigma_z^{i,j}\sigma_z^{i,j+1} + 2\Omega \sigma_x^{i,j} \cos(\omega t). \tag{1.6}$$

By again considering the terms affecting a particular spin in the main body of the lattice ($k(>1), l(>1)$ say) we find for $\omega = \epsilon$ and after moving to a rotating frame and making the rotating wave approximation:

$$\mathcal{H} = J\sigma_z^{k,l}(\sigma_z^{k+1,l} + \sigma_z^{k,l+1} + \sigma_z^{k-1,l} + \sigma_z^{k,l-1}) + ... \tag{1.7}$$

where we do not explicitly write out terms not involving spin (k,l). The microwave is now only resonant for spin (k,l) if it has two neighbour spins in each orientation. For a spin on the edge of the lattice there are an odd number of neighbours so

resonance cannot be achieved in this case. However, applying a second microwave with $\omega = \epsilon - J$ allows resonant flips on the edge if two neighbours are down and one up - and this second field has no effect on the bulk spins.

The spin to be measured is the corner spin ($i = j = 1$) and so would form part of a wider computational apparatus. We may therefore assume that it is a different species with a unique resonant frequency. The dynamics of the whole lattice may then be summarised by three rules (in order of precedence):

1. The corner (test) spin is fixed.

2. An edge spin can flip if it has one of its neighbours up and two down.

3. A body spin can flip if it has two of its neighbours up and two down.

We begin by supposing all spins are initialised in the 'down' state apart from the test spin, which is located in the upper left hand corner of our lattice. We can describe this initial state by choosing two basis elements: $|0\rangle$ when the test spin is down, and $|1\rangle$ when the test spin is up. Using our heuristic rules we can see that these two states do not couple to each other - that $\langle 0| H |1\rangle = 0$. In fact $|0\rangle$ does not couple to any other state, so if we start in the $|0\rangle$ state no amplification occurs, as desired.

1.3   Building a Subspace Basis

We will now seek to construct a basis for the subspace containing our system evolution, by looking at states connected by our Hamiltonian. It will be convenient to represent these states on the nodes of a graph, using the edges to represent non-zero elements of the Hamiltonian.

Our starting point is the state $|1\rangle$, with just the corner spin 'up'. From this position our rules allow two possibilities: either the spin to the right of the corner
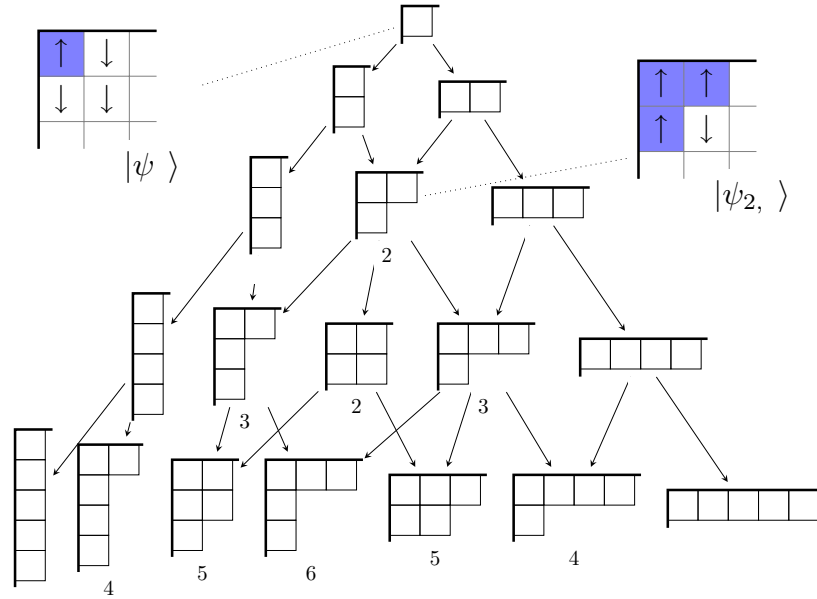
Figure 1.1: Partition states arranged into a lattice. Edges represent a coupling through the Hamiltion of strength Ω. Weights represent the number of different paths through the lattice to a given state.

flips, or the spin below it flips (see Fig. 1.1). In each case, the magnitude of the transition matrix element is Ω. As we continue this procedure, we notice that the states that arise for each excitation number can be characterised by a non-increasing sequence of integers that represent the number of 'up'-spins in each column of the lattice (see Fig. 1.1). Such sequences can also be used to define partitions of at integer: ways of splitting an integer up into a sum of other integers, e.g. $3 = 3 = 2 + 1 = 1 + 1 + 1$. In fact, the states that arise are in 1-to-1 correspondence with such partitions; we call these states 'partition states' and denote them with standard partition notation (see Fig. 1.1). The graph we have just described is depicted in Fig. 1.1 is known as 'Young's lattice' and arises in areas of pure mathematics, such as the representation theory of the symmetric group, and the theory of differential poset. We have drawn weights beneath each state, recording the number of ways the state can be constructed. We will now further reduce the dimension of this basis

by eliminating combinations of states which are inaccessible.

Starting with $|1\rangle$ we see that $\langle 1| H (\alpha_{1,1} |\psi_{1,1}\rangle + \alpha_2 |\psi_2\rangle) = \Omega (\alpha_{1,1} + \alpha_2)$ so $|1\rangle$ does not couple to the two-excitation state $|\psi_{1,1}\rangle - |\psi_2\rangle$. We can eliminate this, leaving a single orthogonal, coupled state with two excitations: $|2\rangle := \frac{1}{\sqrt{2}} (|\psi_{1,1}\rangle + |\psi_2\rangle)$.

We may continue to build up coupled states with larger excitation numbers, and in fact we find that there is only a single coupled state in each case (i.e. we can always eliminate $k - 1$ combinations of partition states with k excitations). To see this, first suppose we have the coupled state with k excitations, which by analogy with the 1D case we write as $|k\rangle$. We can write $|k\rangle = \frac{1}{N_k} \sum_{i \in P(k)} c_i |\psi_i\rangle$, where $P(k)$ is the set of partitions of the integer k and N_k a normalisation factor. We want to construct the state $|k + 1\rangle$ by eliminating the k-dimensional subspace with $k + 1$ excitations, to which $|k\rangle$ does not couple.

Let $|\psi\rangle = \sum_{j \in P(k+1)} \alpha_j |\psi_j\rangle$ and consider the states $|\psi\rangle$ such that

$$0 = \langle k| H |\psi\rangle = \sum_{i \in P(k)} \sum_{j \in P(k+1)} c_i^* \alpha_j \langle \psi_i| H |\psi_j\rangle$$

but $\langle \psi_i| H |\psi_j\rangle = \Omega$ if i is a *parent* of j (a state connect to j, in the lattice row above it), and 0 otherwise, so

$$0 = \langle k| H |\psi\rangle = \sum_{j \in P(k+1)} \alpha_j \sum_{i \in parents(j)} c_i^*.$$

This is the equation of a hyperplane in $|P(k + 1)|$ dimensions, defining the states that are not coupled to $|k\rangle$ through the Hamiltonian. There is a unique single state orthogonal to this hyperplane, $\beta_j = \sum_{i \in parents(j)} c_i$, to which $|k\rangle$ couples. So the only state with $k + 1$ 'up'-spins that $|k\rangle$ couples has coefficients proportional to β_j. After normalisation, we call this state $|k + 1\rangle$.

Unfortunately there is no easy way to write down the partition states and weights

for the nth row of the lattice. Fortunately, for our purposes, we only need to know that the states $|k\rangle$ exist and what the coupling between them is. To find this coupling, consider

$$
\begin{aligned}
g_{n-1,n} &= \langle n| H |n-1\rangle \\
&= \frac{1}{N_{n-1}N_n} \sum_{i\in P(n)} \sum_{j\in P(n-1)} c_i^* c_j \langle \psi_i| H |\psi_j\rangle \\
&= \frac{1}{N_{n-1}N_n} \Omega \sum_{i\in P(n)} c_i^* \sum_{j\in parents(i)} c_j \\
&= \frac{1}{N_{n-1}N_n} \Omega \sum_{i\in P(n)} |c_i|^2 = \Omega \frac{N_n}{N_{n-1}}
\end{aligned}
\tag{1.8}
$$

To find the N_n we need the sum of the squares of the weights of partitions in a given row. A standard result about Young's lattice immediately gives us this sum: $n!$ [12].

This result can be taken straight from the representation theory of the symmetric group: it can be shown that the nodes and their weights represent the irreducible representations and their dimensions. Given that the dimension of each representation is its multiplicity in the regular representation (with dimension $|S_n| = n!$), by dimension counting the result follows. However, for our purposes it is more enlightening to focus on a differetial poset approach, which uses particular combinatorieal features of the lattice to produce the result. Here we give a brief overview of the approach detailed by Sagan in [13].

Let L be an operator that takes a partition state to a sum of its children, and R take a state to the sum of its parents. For example

$$
\begin{aligned}
L |\psi_1\rangle &= |\psi_{1,1}\rangle + |\psi_2\rangle \\
R |\psi_{2,1}\rangle &= |\psi_{1,1}\rangle + |\psi_2\rangle
\end{aligned}
$$

We add a state $|\emptyset\rangle$ such that $L |\emptyset\rangle = |\psi_1\rangle$ and $R |\emptyset\rangle = 0$. Then

$$L^n |\emptyset\rangle = \sum_{i \in P(n)} c_i |\psi_i\rangle \tag{1.9}$$

and

$$R^n L^n |\emptyset\rangle = \sum_{i \in P(n)} |c_i|^2 \tag{1.10}$$

We then need to use two facts about the structure of the lattice: that each element has one more child than it does parents, and each pair of elements either share both a single parent and a single child, or neither. The first of these properties is easy to see: each child corresponds to adding a square at a concave corner of the diagram, and each parent corresponds to removing a convex corner. These corners alternate along the boundary of the shape, starting and ending with concave ones, and so there is always one more child than parents. The second property requires more work, but is roughly because two elements share a parent if, when placed on top of one another they differ by precisely two squares. Taking the union of these shapes you can find the unique child that they also both share.

These properties imply the commutation relation $RL - LR = I$, so

$$R^n L^n |\emptyset\rangle = R^{n-1} L^n R |\emptyset\rangle + n R^{n-1} L^{n-1} |\emptyset\rangle = ... = n! |\emptyset\rangle \tag{1.11}$$

and so, $n! = \sum_{i \in P(n)} |c_i|^2$.

Referring back to Eq. (1.8), and using $N_i = \sqrt{i!}$, we see that

$$\mathcal{H} = \Omega \sum_n \sqrt{n} \left(|n-1\rangle \langle n| + |n\rangle \langle n-1| \right). \tag{1.12}$$

In essence we have established a linear sequence of states, each coupled to the ~~the~~

next analogously to the states on a 1D chain 1.5. However, each of our states is in fact a superposition of many configurations of the 2D array, and crucially the effective coupling from each state to the next increases along the sequence.

1.4   Rate of Spin Propagation

It has been shown (e.g. [14]) that a quantum state released at the end of a semi-inifinite chain of states, with constant couplings, will travel ballistically: the average position of the state along the chain is proportional to the time passed, and inversely proportional to the coupling strength. Since, in the one-dimensional case, the position is proportional to the number of spins that have flipped, we have that the total polarisation will increase linearly with time.

We can establish the rate of propagation in the 2D case using the ansatz that the time taken to travel between two neighbouring nodes is inversely proportional to the strength of the coupling between them. The total time is then $t_{2D} \propto \sum_{i=1}^{n} \frac{1}{\sqrt{i}} \simeq n^{\frac{1}{2}}$. As in the one-dimensional case, the position along the chain corresponds to the the number of spins that have flipped, and so we would expect the total polarisation to be proportional to t^2. This prediction of a quadratic speed-up of signal going from 1D to 2D is the central result of the chapter, and was confirmed by simple numerical simulations of Eq. (1.12) (Fig. 1.2).

1.5   Extension to 3D

Unfortunately the mapping from 2D to 1D is not readily extendible to 3D. However, our results so far could have been anticipated using simple dimensional arguments; if one postulates that the rate of spin propagation is proportional to the boundary of the region, one can predict the correct scaling behaviour. In 1D the boundary
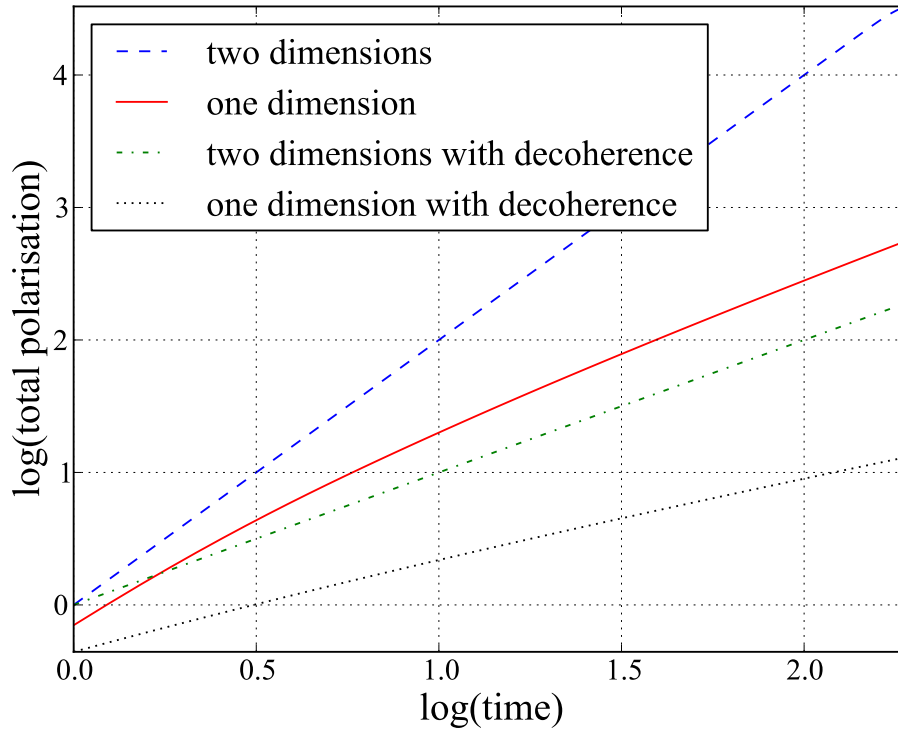
Figure 1.2: Expected total polarisation against time. Time in units of $\frac{1}{\Omega}$, dephasing rate $\Gamma = 1$. The gradient of the 'one dimension with decoherence' line tends to $\frac{1}{2}$ asymptotically.

size is independent of the region size; no matter how many spins have flipped, it still has size one. The coupling strength between states $|n\rangle$ is constant. In the 2D case, the boundary size scales with the square root of the area, and the coupling goes with $\sqrt{n}$. In 3D, the boundary scales like the cube root of the volume squared, and so we expect the coupling to scale as $n^{\frac{2}{3}}$. Following similar logic to that used in 2D case: $t_{3D} \propto \sum_{i=1}^{n} \frac{1}{i^{\frac{2}{3}}} \simeq n^{\frac{1}{3}}$, and so $n \sim t^3$.

1.6 Robustness against Decoherence

We now consider the effect of decoherence. Much of the early work on continuous time quantum random walks looked at the speedup they afforded over their classical

counterparts [15], but didn't make any statement about the conditions under which we would expect the quantum walk to exhibit classical behaviour, as we might expect in a regime of suitably heavy dephasing, say.

We begin by considering a collective noise operator: $L = \sum_n n \, |n\rangle \langle n|$. This represents noise that applies uniformly to the whole lattice: global fluctuations in the magnetic field, for example. As the effect of this type of noise depends only on the number of 'up' spins, the system remains in the reduced basis of number states calculated earlier, with only the coherences between these states affected.

Our starting point is the Lindblad master equation

$$\dot{\rho} = i \, [\rho, H] + \frac{1}{2}\Gamma \left(2L\rho L^\dagger - L^\dagger L \rho - \rho L^\dagger L \right). \tag{1.13}$$

We proceed by splitting up the equation into diagonal and off-diagonal terms

$$\dot{\rho}_{ii} = i \sum_{k=\pm i} \left(\rho_{ik} g_{ki} - \rho_{ki} g_{ik} \right) = -2 \sum_{k=\pm i} Re \, [\rho_{ik} g_{ki}] \tag{1.14}$$

$$\dot{\rho_{ij}} = i \left(\sum_{k=\pm j} \rho_{ik} g_{kj} - \sum_{k=\pm i} \rho_{kj} g_{ik} \right) - \Gamma \rho_{ij} \tag{1.15}$$

where g_{ij} is the coupling between states i and j. In the limit of heavy dephasing ($\Gamma \gg g$), we have a process similar to adiabatic following, and we can make the approximation

$$\Gamma \rho_{ij} \approx i \left(\sum_{k=\pm j} \rho_{ik} g_{kj} - \sum_{k=\pm i} \rho_{kj} g_{ik} \right).$$

We consider the ρ_{ij} as a set of $\frac{n(n-1)}{2}$ variables and solve for them in terms of the ρ_{ii}. Neglecting terms that are second order in $\frac{g}{\Gamma}$, and substituting back into Eq. (1.14) gives

$$\dot{\rho}_{ii} = - \sum_{j=i\pm1} \frac{2|g_{ij}|^2}{\Gamma} \left(\rho_{ii} - \rho_{jj} \right).$$
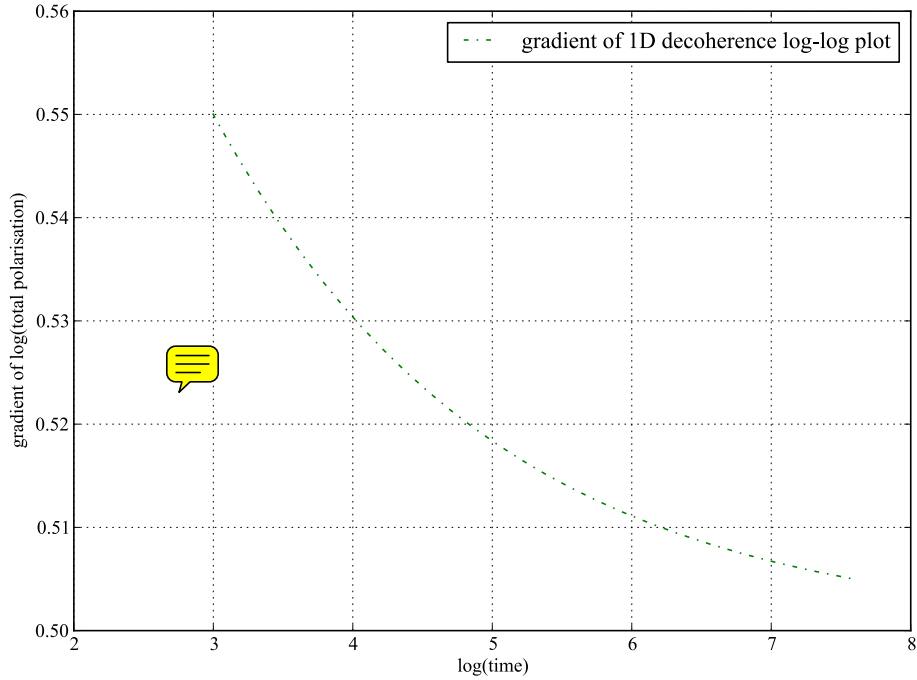
Figure 1.3: The gradient of the 'one dimension with decoherence' line tends to $\frac{1}{2}$ asymptotically.

Our quantum chain formally reduces to a classical Markov chain on the same statespace, with transition rates proportional to the coupling squared. Although states with more 'up' spins decohere more quickly, the decoherence rate Γ is not multiplied for higher states, as it is the *relative* decoherence rate between neighbouring states, which is of importance.

In one-dimension $g_{ij} = 1$ and we are reduced to a simple random walk on a semi-infinite line. By analogy with simple diffusion we expect that the resulting distribution is roughly Gaussian, with the expected number of flipped spins going with $\sqrt{t}$: the rate of spin propagation drops from t to $\sqrt{t}$. This result was confirmed numerically - although (Fig. 1.2) appears to show something closer to a $t^{\frac{2}{3}}$ dependence, (Fig. 1.3) shows that the $\sqrt{t}$ value is recovered as time increases.

In the two-dimensional case $g_{ij} = \sqrt{j}, j = i + 1$: We get a random walk with increasing transition rates. Numerically (Fig. 1.2), we find that the rate of spin

propagation drops from t^2 to t - still an encouraging scaling.

So far we considered a collective noise scenario, using a single Lindblad operator, $L = \sum_n n |n\rangle \langle n|$. This is convenient to analyse for our system, as the system remains in the subspace covered by our basis of number states. A more realistic model involves treating the noise occurring at each site as independent. In this case we have Lindblad operators of the form

$$L_i = \sigma_z^i \tag{1.16}$$

for lattice sites i. Following a similar procedure to before we find the equivalent classical chain to be

$$\dot{\rho}_{ii} = - \sum_{j \in P(i)} \frac{2|g_{ij}|^2}{\Gamma} \left(\rho_{ii} - \rho_{jj} \right) \tag{1.17}$$

where, crucially, the index now runs over all the partition states, rather than our basis of accessible states. In fact, in the 1D case these states are one and the same, and so the spin propagation goes as $\sqrt{t}$, as found in the collective noise case. In the 2D case, we are now performing a continuous-time classical random walk on Young's lattice. We are able to use the property that each node always has one more child than parents, to predict that the rate of spin propagation will be proportional to t - the same as the collective noise case.

1.7 Robustness against Imperfect Initialisation

Finally we consider imperfect inital polarisation (i.e. finite temperature) - a property exhibited by any real experimental system. A fortuitous consequence of the propagation rules is that our system is particularly robust against this source of error; it is difficult for imperfections in the centre of the lattice to spread (Fig. 1.4).

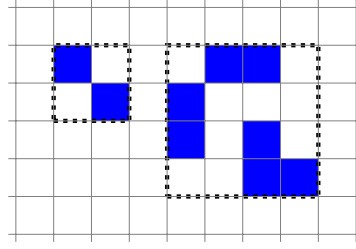To estimate an upper bound for our initialisation threshold we took a randomly

Figure 1.4: Maximum extent of propagation of initialisation imperfections in the lattice - due to propagation rules imperfections are unable to grow beyond the dotted bounding boxes.

initialised lattice, with given imperfection probability, and evolved it using purely deterministic rules, to see whether the imperfections grew to cover over half the lattice. We expect this to give a loose upper bound for the quantum case, as quantum imperfections will both grow and shrink, making it less likely that they will compound in the same manner as deterministic growth. Fig 1.5 shows the results of these simulations; below 4% the probability of growing to cover the majority of the lattice is negligible.
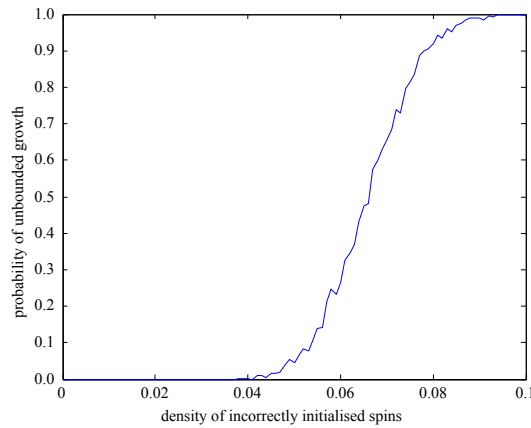

Figure 1.5: Probability that imperfections at given density will deterministically grow to cover over half the lattice.

This threshold places our protocol well within experimental capabilities; for ex-

ample for an array placed in a standard W-band electron spin resonance system
(100 GHz) and cooled using liquid 4He to 1.4 degrees Kelvin, only 3.1% of electron
spins will be in the 'up' state.

1.8   Conclusion

Electron and nuclear spins have been employed in many of the early demonstrations
of quantum technology but applications in real world QT are limited by the difficulty
of measuring single spins. In this chapter we have shown that it is possible to
rapidly and robustly amplify a spin state using a lattice of ancillary spins. The
model we have employed corresponds to an extremely simple experimental system:
a homogenous Ising-coupled spin lattice in one, two or three dimensions, driven by
a continuous microwave field. We have constructed a natural basis for the problem
and used this to assess the rate of amplification, both ideally and in the presence of
environmental noise. We establish that the process can operate at finite temperature
(imperfect initial polarisation) and under the effects of various forms of decoherence.

Chapter 2

Single Photon Source

2.1 Introduction

Single photon sources are an essential component of many quantum information processing (QIP) protocols, from quantum key distribution (QKD) protocols [16, 17] to linear optical quantum computing (LOQC) schemes [18, 19, 20]. Optical schemes using path erasure, a two-photon interference effect, can be used to generate long-range entanglement between physically separated systems [21, 22, 23, 24]. Such procedures can be repeated on many different pairs of systems and so create a distributed cluster state [25, 20], which is the key resource required for implementation of measurement based quantum computing.

In order to be useful in these applications, a photon source must be of a high quality in two respects: it must reliably produce a single photon on demand, and the photons produced must be indistinguishable from one another.

To be perfectly indistinguishable, photons must have the same pulse width, band width, polarization, arrival time at the detector, and carrier frequency. Indistinguishability is vital if photons are to exhibit high quality quantum interference, and its consideration is therefore critical when designing photon sources for LOQC and

path erasure entanglement generation. If photons can be distinguished even in principle, this can lead directly to imperfect LOQC gates, or to a lessening of the degree of entanglement generated in distributed cluster states. In QKD, indistinguishability is less important as interference effects are not required, but it is of paramount importance that no more than one photon is emitted on demand; multiple photon emission leads to security loopholes [20].

As a measure of indistinguishability we exploit the Hong-Ou-Mandel (HOM) effect [26], which relies on the bunching behaviour of identical photons when they are incident on a beam splitter with the same temporal profile. If the photons are indistinguishable, they will always emerge in and be detected in the same output arm (Fig. 2.1). The number of same-arm detection events are usually plotted as a function of arrival time of the two photons - and hence a 'dip' at a time difference of zero is an indicator of indistinguishability. The degree of distinguishability can be
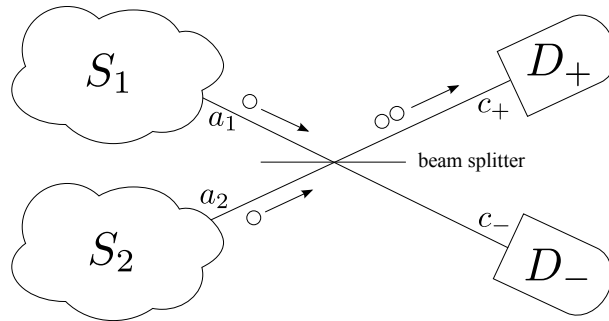

Figure 2.1: Hong-Ou-Mandel effect: a pair of photons from two sources S_1 and S_2 incident on a beam splitter exhibit perfect bunching behaviour if they are completely indistinguishable. In this case the detectors D_+ and D_- will never click simultaneously.

given by the Hong-Ou-Mandel visibility, v_{HOM}, which is the proportion of same-arm detections, over many runs of the experiment. It is worth noting that this definition of v_{HOM} differs from the Hong-Ou-Mandel dip commonly measured in experiments: the typical experimental setup involves continuously pumped systems, and looks for

an absence of simultaneous detections in different detector arms; we consider an on-demand photon pair, and look at the probability that the two detections are in the same arm *over the complete run of the experiment.*

As mentioned above, besides indistinguishability an essential characteristic of a good photon source is that it will consistently produce a single photon, but never more than one, on demand [27]. A laser source can be attenuated so that it gives zero or single photons most of the time. However, photons from classical lasers sources obey Poissonian statistics so that in order to keep the two-photon event rate low the probability of a single photon may become unworkably small for many applications. In addition to this, Poissonian sources are unsuitable for two-photon interference experiments since the rate of two photon production from a single source is similar to that for a single photon from each source [20]. It is worth noting that perfect efficiency should never be a requirement in any realistic optical QIP scheme, as these schemes must always be tolerant to photon loss within other parts of the apparatus. However, a good photon source must be reasonably efficient to be useful, and we should not be forced to trade efficiency for other desirable characteristics.

The use of low-dimensional quantum systems as single photon sources avoids the efficiency problems of Poissonian sources. Successful experimental implementations have been realised in a number of different systems including atom-cavity schemes [28, 29, 30, 31], quantum dots [32, 33] and diamond colour centres [34, 35, 36]. While the majority of the work has been focussed on the efficient production of a single photon, recent experiments in NV centres [35, 36] and quantum dots [37, 38] have demonstrated two-photon interference effects from different sources, albeit sacrificing efficiency by filitering out undesired frequencies. It has been suggested that cavities could be used in these systems, to enhance the emission into the target mode, reducing the need for filtering [39].

In order to improve the characteristics of a photon source, it is not sufficient to

simply consider the material parameters of the system being used: one should also consider the approach used to control the system. Perhaps the simplest strategy is to excite the system first optically, either coherently or incoherently, and wait for the system to relax into its ground state, emitting a photon in the process; we will henceforth refer to this as the 'pulse-relax' technique. This approach makes minimal resource demands on the system and, due to its simplicity, is the technique proposed in some remote entanglement generation schemes [21, 23]. The pulse-relax approach is problematic in systems where the excited state is sensitive to decoherence, which will degrade the photon's indistinguishability [40, 41, 21, 42]. These effects can be reduced, for example by exploiting the Purcell effect to enhance the emission rate into the desired photon mode [43, 44] or by using temporal post-selection of emitted photons [42]. However with experimental limits on cavity couplings both of these inevitably lead to lower efficiency as the proportion of emissions that are utilized falls [45].

A fundamentally different approach is to use more elaborate QED schemes to release a photon from the system in a controlled manner. In particular single photon sources using a Raman approach have been analysed [40, 41] and experimentally realised [28]. The approach places more demands on the system, requiring a three level system with a Λ-system configuration. Each arm is coupled to either a classical or a quantum light field; in Fig 2.2 we show the situation when one arm is driven classically, with a coupling Ω, and the other arm is coupled to a cavity mode with strength h. By detuning both arms of the Λ-system by the same amount ν, population is transferred from one arm to the other, whilst suppressing population in the top state. Provided that the coupling strengths are small in comparison to the detuning, $\Omega \ll \nu$ and $h \ll \nu$, we induce an effective coupling between the two low-lying states, which causes oscillations with Rabi frequency $h\Omega/4\nu$. The population in the excited state remains small at all times, and so any decoherence that
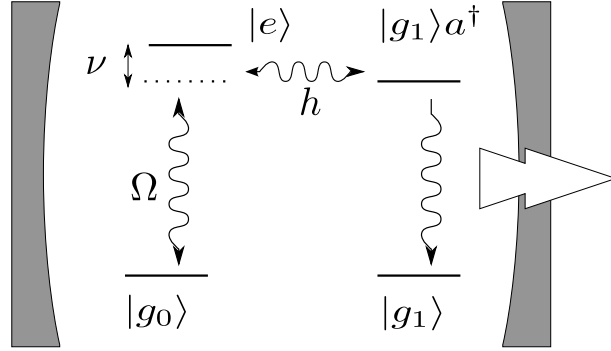
Figure 2.2: Effective level structure of a driven $\Lambda-$system inside an optical cavity. Here, Ω is the amplitude of an external (laser) driving field, h the optical dipole-cavity-coupling, and ν the shared detuning of the laser and the cavity transition frequency from the excited state. The system can decay into state $|g_1\rangle$ and in doing so emit a photon into a well-defined external mode.

arises due to environmental coupling to this excited state may be reduced using this strategy. In particular, a common realisation of a single photon source is a quantum dot, in which the excited state typically has a different charge configuration to the ground state. This causes local lattice distortions, which in turn locally alter the electronic bandgap, thus inducing a coupling to acoustic phonons [46, 47] that can act as a noise source.

In this ~~paper~~ we provide a detailed and realistic analysis of the effects of the lattice vibrations for single photon emitters based on (self-assembled) semiconductor quantum dots. By comparing a standard pulse-relax approach with the aforementioned Raman technique, we find that the latter can can offer considerable improvements in terms of both photon indistinguishability and source efficiency. Our results extend and complement a previous study [41] which considered generic pure dephasing noise. However, here we also show that the precise choice of control parameters is important if phonon-induced decoherence is to be successfully suppressed.

2.2 Our model

For convenience of notation we consider the Λ-system detailed in Fig. 2.2 for both the pulse-relax and the Raman approach. In both cases one arm of the system is coupled to the cavity with detuning ν. In the Raman scheme, the other arm is driven with strength Ω by a laser with a matching detuning ν, and the system starts in state $|g_0\rangle$. By contrast, we model the pulse-relax approach by setting $\Omega = \nu = 0$ and starting in state $|e\rangle$, ignoring the details of the excitation process. The fact that we are neglecting the excitation step in this simplified picture will slightly favour the pulse-relax approach, but is largely justified on the assumption that the initial excitation process takes place quickly compared with other system dynamics. Our framework thus allows us to consider the pulse-relax approach as a special case of the master equation we will now derive for the Raman approach.

We split the Hamiltonian into contributions from the emitter system and cavity (sys), the driving laser (dr), the unperturbed phonon bath (ph) and interaction terms between the system and phonon bath ($sys - ph$), system and target external mode ($sys - mod$), and system and other exernal modes ($sys - ext$):

$$H = H_{sys} + H_{dr} + H_{ph} + H_{sys-ph} + H_{sys-mod} + H_{sys-ext} \ . \tag{2.1}$$

The $H_{sys-mod}$ and $H_{sys-ext}$ terms are well understood, and we will treat these by adding in the appropriate Lindblad terms to our final master equation. In the following, we shall describe the rest of these terms separately.

Using the standard Jaynes-Cummings Hamiltonian, the Λ-system coupled to a cavity mode with strength h and detuning ν from resonance can be described by the following Hamiltonian:

$$H_{sys} = (\omega + \nu) |e\rangle \langle e| + \omega a^\dagger a + \frac{h}{2} \left(|g_1\rangle \langle e| a^\dagger + \text{h.c.} \right) \ , \tag{2.2}$$

where h.c. denotes the Hermitian conjugate. ω is the cavity mode frequency.

We can restrict ourselves to one or zero cavity photons since the Jaynes-Cummings model preserves excitation number and after photon emission we assume that the emitter system remains in state $|g_1\rangle$ - i.e. we make the approximation that once a photon has escaped re-excitation does not occur - at least until an appropriate reset step (such as thermal relaxation) which we assume happens on a much longer timescale than the photon emission dynamics. This allows us to replace $|g_1\rangle a^\dagger$ with a new combined atom-photon state $|g_a\rangle$ and $a^\dagger a$ with $|g_a\rangle\langle g_a|$.

The term H_{dr} describes a laser driving the transition $|g_0\rangle \leftrightarrow |e\rangle$ with coupling strength Ω, and whose frequency is detuned from resonance by the same ν parameter, yielding

$$H_{dr} = \Omega \cos(\omega t) \left(|e\rangle\langle g_0| + \text{h.c.}\right) \ . \tag{2.3}$$

After performing the rotating wave approximation, assuming that $\omega \gg \nu, h, \Omega$, we are left with

$$H_{sys} + H_{dr} = \nu |e\rangle\langle e| + \frac{1}{2}\left(h|g_a\rangle\langle e| + \Omega|e\rangle\langle g_0|\right) + \text{h.c.} \tag{2.4}$$

for the total system Hamiltonian.

We model the phonons as a bath of harmonic oscillators

$$H_{ph} \quad = \sum_q \omega_q b_q^\dagger b_q, \tag{2.5}$$

which couple to the exciton state $|e\rangle$ through the deformation coupling with coupling

constants $f_q = D|q|$ in the usual way [47]:

$$H_{sys-ph} = |e\rangle \langle e| \sum_q f_q \left(b_q^\dagger + b_q\right). \tag{2.6}$$

The effect of the phonon bath on a driven quantum dot can be described using a Lindblad master equation [48], where the Lindblad operators induce phonon-assisted transitions between the dressed system eigenstates [49]. Being analogous to Refs [48, 49], it suffices to outline the derivation of the phonon master equation only briefly in the following. To derive the master equation we must first diagonalise the system Hamiltonian, $H_{sys} + H_{dr}$. We find that the eigenvalues are

$$
\begin{aligned}
\lambda_0 &= 0, \\
\lambda_\pm &= \frac{\nu \pm \sqrt{\nu^2 + \Omega^2 + h^2}}{2},
\end{aligned}
\tag{2.7}
$$

with corresponding eigenvectors

$$
\begin{aligned}
|\psi_0\rangle &= n_0 \left(h |g_0\rangle - \Omega |g_a\rangle\right), \\
|\psi_\pm\rangle &= n_\pm \left(\Omega |g_0\rangle + h |g_a\rangle + 2\lambda_\pm |e\rangle\right).
\end{aligned}
\tag{2.8}
$$

n_0 and $n_\pm$ are appropriate normalisation factors. We now make the Born and Markov approximations which lead to the master equation [50] in standard Lindblad form:

$$\dot{\rho} = i\left[\rho, H\right] + D_{ph}(\rho) \tag{2.9}$$

with the phonon dissipator given by

$$D_{ph}(\rho) = J(\Lambda) \left[(N(\Lambda) + 1) D\left[P_\Lambda\right] \rho + N(\Lambda) D[P_\Lambda^\dagger]\rho\right] \tag{2.10}$$

where $D[L]\rho = L\rho L^\dagger - 1/2(L^\dagger L\rho + \rho L^\dagger L)$, $\Lambda = \lambda_+ - \lambda_-$, and $P_\Lambda = -\left|\psi_-\right\rangle\left\langle\psi_+\right|$. Note that the phonons only induce transitions between the two optically bright system eigenstates and do not couple to the dark $\left|\psi_0\right\rangle$. In the above equation $N(\Lambda)$ is the bosonic mode occupation number:

$$N(\omega) \quad = \frac{1}{e^{\beta\omega}-1} \tag{2.11}$$

$\beta = (k_B T)^{-1}$ and we shall be henceforth consider all systems at room temperature, $T = 298$ K. The spectral density function $J(\omega)$ represents the electron-phonon coupling weighted by the density of phonon modes [50]. We expect this to be dominated by deformation potential coupling, and in this case we obtain [48]:

$$J(\omega) \quad = \alpha\omega^3 e^{-\left(\frac{\omega}{\omega_c}\right)^2} . \tag{2.12}$$

We take $\alpha = 0.0027$ ps^{-1} and $\omega_c = 2.2$ ps^{-1}, values that agree well with experiments on self-assembled quantum dots [46, 51].

We absorb the rates in (2.10) into the Lindblad operators to obtain following decoherence operators:

$$U_+ \quad = \sqrt{J(N+1)}\left|\psi_-\right\rangle\left\langle\psi_+\right| \tag{2.13}$$

$$U_- \quad = \sqrt{JN}\left|\psi_+\right\rangle\left\langle\psi_-\right| \tag{2.14}$$

where we have taken $J = J(\Lambda)$ and $N = N(\Lambda)$. Note that if non-Markovian dynamics are taken into account [52] this can lead to effects on the ultra-short timescale, but these are in general much shorter than typical dynamics studied here.

As a measure of the degree of indistinguishability of the photons produced in the emission process, we consider the HOM visibility, which is the normalised probability

of same arm detections obtained over many runs of the experiment,

$$v_{\text{HOM}} = \frac{p_{\text{same}} - p_{\text{diff}}}{p_{\text{same}} + p_{\text{diff}}}, \tag{2.15}$$

where $p_{\text{same}} = p(D_+ \cap D_+) + p(D_- \cap D_-)$ and $p_{\text{diff}} = p(D_+ \cap D_-) + p(D_- \cap D_+)$ with $p(D_x \cap D_y)$ being the probability of obtaining a click in detector D_y followed by a click in detector D_x.

In order to calculate v_{HOM} we thus need to consider photons emitted from two copies of the system S_1 and S_2, one for each input arm of the beam splitter interferometer. The joint state of the system then inhabits the space $S = S_1 \otimes S_2$ (Fig. 2.1). We label the two cavity modes using annihilation operators a_1 and a_2. Using the input-output formalism (e.g [53]) and neglecting incoming light, we can describe the modes outside the cavities as $a_{i,out} = \sqrt{}$ here κ is the cavity leakage rate. The modes corresponding to detection in $D_\pm$ are labelled $c_\pm$ respectively. Due to the transformation performed by the beam splitter, $c_\pm$ can be written in terms of a_1 and a_2 as follows:

$$c_+ = \sqrt{\kappa}\frac{1}{\sqrt{2}}\left(a_1 + a_2\right), \tag{2.16}$$

$$c_- = \sqrt{\kappa}\frac{1}{\sqrt{2}}\left(a_1 - a_2\right). \tag{2.17}$$

We assume that the field in the mode outside the cavity is directly related to the field inside, neglecting the process of escape from the cavity. The effect on the system $S = S_1 \otimes S_2$ of a detection in the plus or minus output mode is then described by the projection operators

$$C_\pm = |g_1\rangle\langle g_a| \otimes \mathbf{1} \pm \mathbf{1} \otimes |g_1\rangle\langle g_a|. \tag{2.18}$$

We could now simulate many trajectories of this system and build up an estimate

of v_{HOM} by averaging these [54]. Instead we introduce a technique that we call the *semi-quantum master equation* method, which will allow us to find v_{HOM} in a single run of a master equation acting on a slightly larger Hilbert space.

2.3 Introducing the Semi-Quantum Master Equation Method

We are often interested in 'observable events' in quantum systems, such as the emission of a photon. When an event is observed the system undergoes a transition due to wave function collapse. During a period when no event is observed the system evolves according to a conditional master equation, reflecting the fact if events could be observed but are not, then this also informs our knowledge of the state. In order to answer questions about the probabilities and time distributions of events or chains of events, one approach is to use a quantum jump master equation to generate individual trajectories of the system. In each timestep we decide probabilistically whether an event should occur. If it does occur then the system collapses according to a quantum jump; if it does not occur then the system evolves conditioned on no jump occurring. Statistics about the quantities of interest are built up as many trajectories are created.

Here we look at a different approach to calculating the quantities relating to events that occur in such systems. Instead of simulating multiple trajectories of the system, we efficiently increase the size of the statespace to record the information of interest. This allows us to calculate the desired system properties, and their time evolution, by solving a single master equation.

Consider a system that can exist in a number of different states. Let a movement between these states constitute an event, and assume that each kind of event happens

at a given rate. Such a system is heavily reminiscent of a classical continuous time Markov chain (CTMC), which can be represented as a graph with the states as nodes and the edges events weighted by the transition rates (Fig. 2.3). Given an
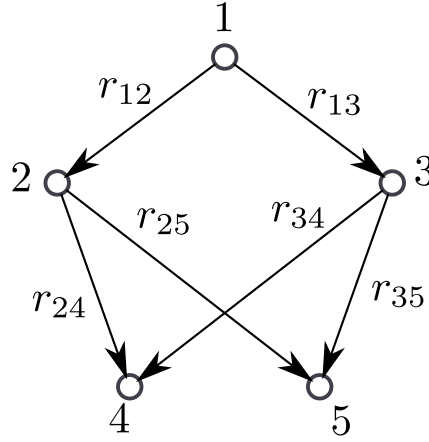

Figure 2.3: A classical continuous-time Markov chain, with statespace $W = \{1, 2, 3, 4, 5\}$. The edge weight, r_{ij}, represents the transition rate from state i to state j. If $\rho_i(t)$ is the population in state i at time t, the system is governed by the rate equations $\dot{\rho}_i = \sum_{j \in W} r_{ji}\rho_j$.

initial state i in a chain of size n, we can calculate the probability that at a later time t the chain is in state j, by solving the rate equations - a set of n ordinary differential equations.

Quantum systems differ from classical continuous-time Markov chains due to quantum superposition. We are not able to simply record the population in each quantum state as inter-state coherences are also important. Using a Markov chain to model the whole quantum system is not possible by definition - systems that can be modelled in this way do not exhibit quantum behaviour.

In what follows it is helpful to explain carefully what we mean by 'state'. In quantum systems a state is usually a vector in the Hilbert space of the system. We shall call this a quantum-state. We can also refer to the 'state' of the overall process, considering for example a system that has emitted a photon to be in a

different process-state to one which has not. A system changes process-state when an event is observed.

Whereas thinking in terms of the CTMC is not useful when considering quantum-states, it is an effective way to think about process-states. As process-states are separated by an observed event, no coherences can exist between the two histories, making a CTMC approach feasible. Of course, process-states alone are not enough to model the whole system. Each process-state needs its own copy of the system attached to it. We can think of a Markov chain with a copy of our system at each node, where the transition rates are determined by the jump Lindblad operators corresponding to the events. Another way of thinking about this is that we extend our overall space with a set of process-states, to allow us to record events in the system.

Formally, we take a set of process-states S_P, transitions between which corre-spond to our observable jump events described by jump operators $J_Q^{(i)}$. We extend the Hilbert space of our quantum system S_Q by forming the tensor product:

$$S = S_Q \otimes S_P. \tag{2.19}$$

The new Hamiltonian is given by

$$H = H_Q \otimes \mathbf{1}. \tag{2.20}$$

If event $J_Q^{(i)}$ causes a transition from system state a to b we say it is of type (a, b). Its action on the extended system S is described by

$$J^{(i)} = J_Q^{(i)} \otimes |b\rangle \langle a| . \tag{2.21}$$

For any other Lindblad operators acting on the system $L_Q^{(i)}$, we need to create a set

of size $|S_P|$ Lindblad operators - one to operate on each subspace independently:

$$s(L_Q^{(i)}) = \left\{ L_Q^{(i)} \otimes |j\rangle \langle j| , j \in S_P \right\}. \tag{2.22}$$

At first glance it might appear that we have increased a system of size $m = |S|$ to size mn, where $n = |S_P|$. Whilst this is true, the situation is not as bad as it seems at first, because the coherences between the different subsystems are unimportant – instead of a density matrix of size $(nm)^2$ we can use a system of size nm^2, an increase linear in the number of system states. In practice we can often do better than this by eliminating unnecessary states from some of the subsystems.

As a simple concrete example, consider a resonantly driven two-level system $S_Q = \{|g\rangle, |e\rangle\}$, with Hamiltonian

$$H_Q = \Omega \left(|g\rangle \langle e| + |e\rangle \langle g| \right). \tag{2.23}$$

Suppose that it is also possible for the system to spontaneously emit from state $|e\rangle$ into the environment - a transition described by the jump operator

$$J_Q = |g\rangle \langle e|. \tag{2.24}$$

We are interested in knowing about the time distribution of the first time a photon is emitted. We add the two process-states 0 and 1, indicating whether the event has occurred or not. Our new system is described by:

$$S = \{ |g0\rangle, |e0\rangle, |g1\rangle, |e1\rangle \} \tag{2.25}$$

$$H = \Omega \left(|g0\rangle \langle e0| + |e0\rangle \langle g0| + |g1\rangle \langle e1| + |e1\rangle \langle g1| \right) \tag{2.26}$$

$$J_1 = |g1\rangle \langle e0| \tag{2.27}$$

$$J_2 = |g1\rangle \langle e1|. \tag{2.28}$$

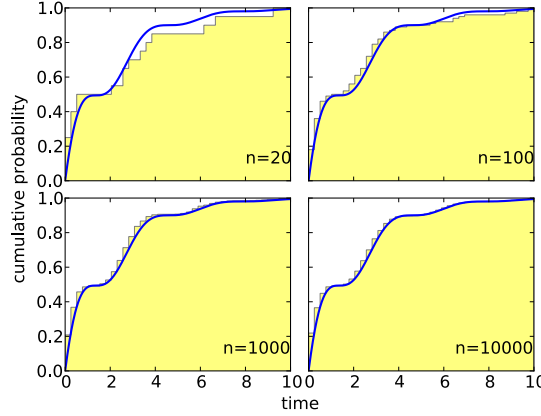The population in the 1 subspace at time t will give us the probability a photon has been emitted by this time.

Figure 2.4: Comparison of semi-quantum master equation approach with Monte Carlo simulations of n=20, 100, 1000, and 10000 runs, for the system described by 2.25- 2.28. For the cumulative histogram plots we used horizontal binning with 40 bins, which explains why the horizontal resolation does not improve further for the larger values of n.

If we only cared about this distribution, we could reduce the size of the system by replacing the states $|g1\rangle$ and $|e1\rangle$ with a single state $|1\rangle$ to keep track of the cumulative jump probability over time. We would need to remove the last two terms from the Hamiltonian as well as J_2, and set $J_1 = |1\rangle\langle e0|$. Figure 2.4 shows the cumulative jump probability for this system, showing agreement between the SQME results and Monte Carlo simulations with increasing numbers of runs.

2.4 Applying the Semi-Quantum Master Equation Method

When calculating v_{HOM} we must consider events in which photons trigger either detector, and events in which photons are spontaneously emitted into the environ-
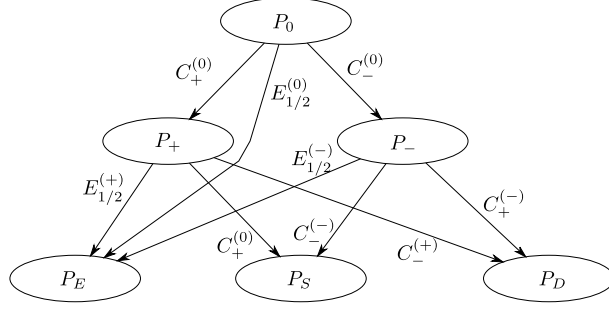
Figure 2.5: The system jump-space: On the first jump the system moves to P_+/P_- depending on the arm in which the photon is detected. After the second jump the system moves to state P_S/P_D depending on whether the second photon was detected in the same or different arm to the first. At any point the system can undesirably spontaneously emit into the environment, moving to the junk state P_E.

ment. We introduce a set of process-states to record and labels these event classes (Fig. 2.5):

$$S_P = \{P_0, P_+, P_-, P_S, P_D, P_E\}. \tag{2.29}$$

The process-state starts as P_0 and remains there until an event of interest occurs. $P_{+/-}$ represents the process-state after a single photon has been detected in the $D_{+/-}$ detectors respectively. After a second photon has been detected the process-state becomes $P_{S/D}$ depending on whether the second photon was detected in the same or different detector as the first. If at any point a photon is emitted into the environment the process moves to state P_E. When calculating the indistinguishability we can then ignore any population in state P_E, but we must include it when considering the overall efficiency of the process.

We must also identify the operators that cause the movement between the process-states. Before doing this we extend the state-space S of the system to include the process-states:

$$S \;\; = S_1 \otimes S_2 \otimes S_P. \tag{2.30}$$

The detection operators are then given by

$$C_+^{(0)} = C_+ \otimes |P_+\rangle \langle P_0| \tag{2.31}$$

$$C_+^{(+)} = C_+ \otimes |P_S\rangle \langle P_+| \tag{2.32}$$

$$C_+^{(-)} = C_+ \otimes |P_D\rangle \langle P_-| \tag{2.33}$$

$$C_-^{(0)} = C_- \otimes |P_-\rangle \langle P_0| \tag{2.34}$$

$$C_-^{(-)} = C_- \otimes |P_S\rangle \langle P_-| \tag{2.35}$$

$$C_-^{(+)} = C_- \otimes |P_D\rangle \langle P_+| \tag{2.36}$$

where for example $C_+^{(-)}$ is the jump operator representing a second detection in the D_+ detector, when the first detection was in D_-. The spontaneous emission operators are given similarly:

$$E_1^{(0)} = |g_1\rangle \langle e| \otimes \mathbf{1}_S \otimes |P_E\rangle \langle P_0| \tag{2.37}$$

$$E_2^{(0)} = \mathbf{1}_S \otimes |g_1\rangle \langle e| \otimes |P_E\rangle \langle P_0| \tag{2.38}$$

$$E_1^{(+)} = |g_1\rangle \langle e| \otimes \mathbf{1}_S \otimes |P_E\rangle \langle P_+| \tag{2.39}$$

$$E_2^{(+)} = \mathbf{1}_S \otimes |g_1\rangle \langle e| \otimes |P_E\rangle \langle P_+| \tag{2.40}$$

$$E_1^{(-)} = |g_1\rangle \langle e| \otimes \mathbf{1}_S \otimes |P_E\rangle \langle P_-| \tag{2.41}$$

$$E_2^{(-)} = \mathbf{1}_S \otimes |g_1\rangle \langle e| \otimes |P_E\rangle \langle P_-| \tag{2.42}$$

where here $E_1^{(+)}$ represents a emission from S_1 acting after the first photon was detected in the D_+ detector.

Finally we must modify our phonon decoherence operators. The subspaces corresponding to different process-states, are classically separated by observable events. These classically separated branches cannot exhibit interference, and we can there-

fore take the decoherence processes to occur independently on each branch:

$$U_{+,1}^{(0)} = \sqrt{J(N+1)} \,|\psi_-\rangle\langle\psi_+| \otimes \mathbf{1}_S \otimes |P_0\rangle\langle P_0| \tag{2.43}$$

$$U_{-,1}^{(0)} = \sqrt{JN} \,|\psi_+\rangle\langle\psi_-| \otimes \mathbf{1}_S \otimes |P_0\rangle\langle P_0| \tag{2.44}$$

$$U_{+,1}^{(+)} = \sqrt{J(N+1)} \,|\psi_-\rangle\langle\psi_+| \otimes \mathbf{1}_S \otimes |P_+\rangle\langle P_+| \tag{2.45}$$

$$U_{-,1}^{(+)} = \sqrt{JN} \,|\psi_+\rangle\langle\psi_-| \otimes \mathbf{1}_S \otimes |P_+\rangle\langle P_+| \tag{2.46}$$

$$U_{+,1}^{(-)} = \sqrt{J(N+1)} \,|\psi_-\rangle\langle\psi_+| \otimes \mathbf{1}_S \otimes |P_-\rangle\langle P_-| \tag{2.47}$$

$$U_{-,1}^{(-)} = \sqrt{JN} \,|\psi_+\rangle\langle\psi_-| \otimes \mathbf{1}_S \otimes |P_-\rangle\langle P_-| \tag{2.48}$$

with similar operators acting on the second system. We do not need decoherence operators acting on the P_S, P_D or P_E, since we are only concerned with populations in, and not coherences between, these states. Moreover, we only really need to keep track of the total population in each of these subspace, and not the populations of each state that make up each subspace - a fact that we exploit to reduce the dimension of our problem for the numerical simulations.

We form a Lindblad master equation using these 24 Lindblad operators:

$$\dot{\rho} = i\,[\rho, H] + \sum_i \gamma_i \left(L_i \rho L_i^\dagger - 1/2(L_i^\dagger L_i \rho + \rho L_i^\dagger L_i) \right). \tag{2.49}$$

The γ_i are the rates for each process. As noted earlier for the $U_{\pm,i}^{(j)}$ this rate is 1, as the rates have been incorporated into the Lindblad operators. For the $C_\pm^{(i)}$ we need $\gamma = \kappa$, the cavity leakage rate, which we take to be $3h$, a choice that allows for a reasonable enhancement of photon emission from the emitter system into the desired mode outside of the cavity, whilst preventing cavity photons being reabsorbed by the emitter system. For the $E_i^{(j)}$ we take $\gamma = 0.005ps^{-1}$, assuming a radiative livetime of 200 ps. Our model allows only for spontaneous emission directly from the excited state $|e\rangle$; we assume that there is no loss from the cavity to modes other

than the target waveguide mode, and that all photons that are emitted into the target mode are detected. For similar cavities we expect these effects to impact the two approaches to equal extent.

The dimension of this extended space S is $4 \times 4 \times 6 = 96$. In fact we can reduce this by eliminating some unneccessary states from the subspaces. By carefully considering the basis states accessible in each the subspace corresponding to each process, we can reduce the number of system states to $9 + 6 + 6 + 1 + 1 + 1 = 24$. For our simulation we will need to calculate the density matrix for this system. As noted in ... no coherences can exist between the different process-state subspaces. This reduces the number of density matrix elements we need to track to $9^2 + 6^2 + 6^2 + 1 + 1 + 1 = 116$.

2.5 Results

Fig. 2.6 shows the HOM visibility obtained from, and spectral density used in, simulations of the pulse-relax technique. At low coupling strengths the phonon spectral density is small, and so phonon decoherence is largely avoided giving high indistinguishability. As described earlier, we have fixed κ, the cavity leakage rate, to be $3h$ so the effective coupling to the the target mode is proportional to the Purcell factor $h^2/\kappa \sim h$. This means that, for small h, the rate of photon emission into the cavity mode is slow and thus spontaneous emission into environmental optical modes is a problem. To take account of this effect, we define the 'combined HOM visibility', which is the product of success probability and bare HOM visibility, which approaches zero as $h \to 0$. Taking large coupling strengths allows one to access the region to the higher frequency side of the hump in the phonon spectral density and so could avoid this problem, but is unrealistic given the cavity parameters currently obtainable experimentally. In the experimentally feasible region ($h < 1$) [55] we
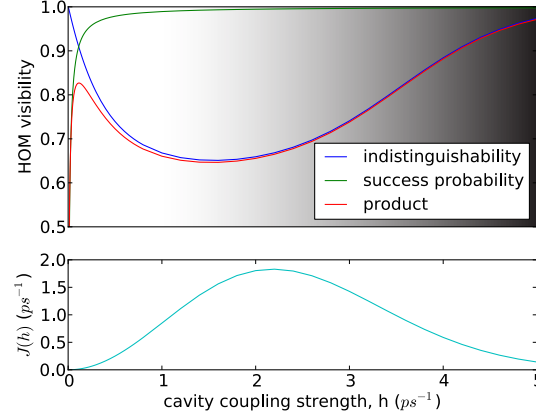
Figure 2.6: Pulse-relax technique: calculations are performed as a function of the cavity coupling strength. Upper panel: at realistic coupling strengths ($h < 1$) increased HOM indistinguishability necessarily entails a decrease in efficiency (success probability), with the product of the two (blue curve) approaching zero. Here the spontaneous emission rate is $\Gamma = 0.005$ ps^{-1}. For overcoming phonon-induced decoherence and achieving a high success probability, we must move into a region of unrealistically high h, represented by the increasing level of shading of this plot. The lower panel shows the phonon spectral density, Eq. 2.12, evaluated at the cavity coupling strength h, giving a rate that is directly proportional to phonon-induced dephasing during the pulse-relax process.

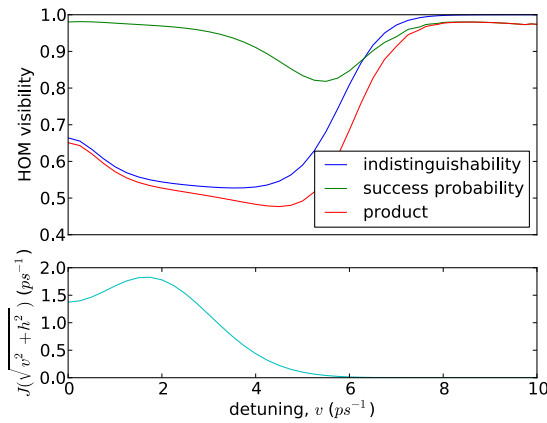must therefore trade indistinguishability for efficiency.

Figure 2.7: Raman technique, $h = 0.5$: by choosing a detuning to move beyond the region of high phonon spectral density we can achieve near-perfect indistinguishability. The efficiency in this region is high enough for a feasible photon source.

In contrast, the Raman procedure (Fig. 2.7) avoids this trade-off. For small detuning the visibility is low, but this is because we do not get a proper Raman ground state transition unless $\nu \gg h$. If this condition is not met, the system simply undergoes a non-optimal detuned pulse-relax transition. Once we reach a detuning of around $\nu = 12h(= 6~\text{ps}^{-1})$ the indistinguishability and efficiency both increase. Our choice of detuning size is limited in that it must be small in comparison with the original energy gap between the ground and excited states, and that it avoids any nearby excited states. This leaves us some freedom to use large detunings to push to frequencies above the region of high phonon spectral density. As the detuning is increased the efficiency saturates below unity. In this region both the time taken for the Raman process and the average excited state lifetime scale with the detuning squared, the two effects cancelling one another.

In many applications where photons are used, the product of efficiency and indistinguishability may not be the most useful metric for characterising the performance of the source; often photon escape errors can be accounted for, and the indistinguishability of photons that are detected is the important figure of merit. We therefore also calculate the rate of production of pairs of photons of a given indistinguishability using each approach (Fig. 2.8). For our production rate we take

$$r_f = \frac{e_f}{t_f} \tag{2.50}$$

where e_f is the efficiency and t_f is the time taken for 99% of the runs to have completed (possibly unsuccessfully), for parameters (h in the pulse-relax scheme, and ν in the Raman scheme) chosen to obtain a given indistinguishability, f. This figure is somewhat approximate as it takes no account of how successful runs (where two photons are emitted into the correct modes) and unsuccessful runs are distributed within the process run time, and no allowance is made for time taken to reset the
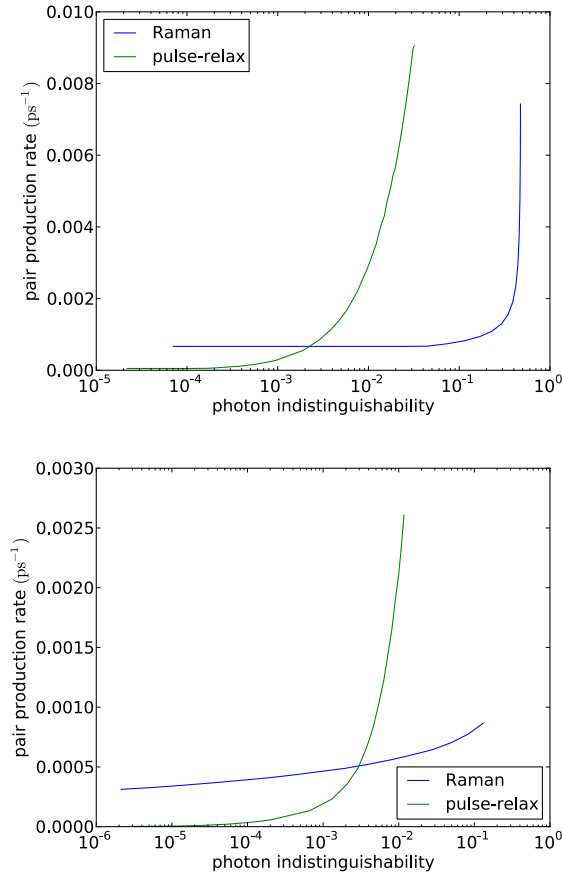
Figure 2.8: Rate of photon pair production: with no spontaneous emission (upper), and spontaneous emission with an excited-state lifetime of 200 ps (lower)

system in the event of a failure. The effect of the former is minor since in our model spontaneous emission can occur uniformly at any point of the process. We will revisit the effect of the latter shortly.

Even in the absence of spontaneous emission (Fig. 2.8, upper panel), the Raman procedure is quicker than the pulse-relax process at generating photons of a sufficiently high level of indistinguishability. With the dephasing parameters chosen in our model this occurs for indistinguishability of greater than 99.9%. In our model, spontaneous emission is the only process degrading the efficiency – without it we have perfect efficiency and so neither of the potential shortcomings discussed in the

previous paragraph apply.

When spontaneous emission is added, we see a similar pattern but the indistinguishability threshold is very slightly lower. This is an upper bound, as here the reset time becomes important. The efficiency of the Raman procedure remains fixed at about 80%, requiring on average 1.25 runs per pair. In contrast, the efficiency of the pulse-relax procedure heads towards zero, meaning that many attempts will be needed to produce a pair. If the time taken to reset the system (to the excited state $|e\rangle$ in which we have assumed the pulse-relax system starts) is large, the Raman procedure will become advantageous at a far lower threshold.

2.6 Conclusion

To conclude, we have developed a realistic and microscopically justified model of the impact of phonons on solid state single photon sources. We used a modified, 'semi-quantum', master equation method for the efficient calculation of coincidence rates, without having to resort to a quantum Monte-Carlo simulation approach.

Our physical results are best summarised by considering the following scenario: suppose you are working with a system where phonon dephasing and spontaneous emission are the dominant loss channels, where you have some control over the cavity parameters (h and κ), and that you are tasked with building a high indistinguishability, efficient, on-demand photon source. In this scenario, we find that a Raman technique is preferable to the pulse-relax approach. In particular, in addition to producing superior production rates at a given indistiguishability, the Raman approach we have taken only requires varying of the detuning - by tuning the cavity mode, and driving field - whilst leaving the other cavity properties fixed. This is in contrast in to the pulse-relax approach that we used for comparison where we allowed the cavity coupling strength itself to be varied within a realistic range of

values.

2.7   Acknowledgements

.1   Semi-quantum Master Equations

Bibliography

[1] CleuziouJ. P., WernsdorferW., BouchiatV., OndarcuhuT., and MonthiouxM. Carbon nanotube superconducting quantum interference device. *Nat Nano*, 1(1):53–59, 10 2006.

[2] F Jelezko, T Gaebel, I Popa, A Gruber, and J Wrachtrup. Observation of coherent oscillations in a single electron spin. *Physical Review Letters*, 92(7):076401, Jan 2004.

[3] Philipp Neumann, Johannes Beck, Matthias Steiner, Florian Rempp, Helmut Fedder, Philip R. Hemmer, Jörg Wrachtrup, and Fedor Jelezko. Single-shot readout of a single nuclear spin. *Science*, 329(5991):542–544, 07 2010.

[4] Andrea Morello, Jarryd J Pla, Floris A Zwanenburg, Kok W Chan, Kuan Y Tan, Hans Huebl, Mikko Möttönen, Christopher D Nugroho, Changyi Yang, Jessica A van Donkelaar, Andrew D C Alves, David N Jamieson, Christopher C Escott, Lloyd C L Hollenberg, Robert G Clark, and Andrew S Dzurak. Single-shot readout of an electron spin in silicon. *Nature*, 467(7316):687–691, Jul 2010.

[5] A. N. Vamivakas, C. Y. Lu, C. Matthiesen, Y. Zhao, S. Falt, A. Badolato, and M. Atature. Observation of spin-dependent quantum jumps via quantum dot resonance fluorescence. *Nature*, 467(7313):297–300, 09 2010.

[6] J Berezovsky, M. H Mikkelsen, N. G Stoltz, L. A Coldren, and D. D Awschalom. Picosecond coherent optical manipulation of a single electron spin in a quantum dot. *Science*, 320(5874):349–352, Apr 2008.

[7] D. Leibfried, R. Blatt, C. Monroe, and D. Wineland. Quantum dynamics of single trapped ions. *Rev. Mod. Phys.*, 75:281–324, Mar 2003.

[8] R. Hanson, L. P. Kouwenhoven, J. R. Petta, S. Tarucha, and L. M. K. Vandersypen. Spins in few-electron quantum dots. *Rev. Mod. Phys.*, 79:1217–1265, Oct 2007.

[9] John J. L. Morton and Brendon W. Lovett. Hybrid solid-state qubits: The powerful role of electron spins. *Annual Review of Condensed Matter Physics*, 2(1):189–212, 2013/04/07 2011.

[10] Jae-Seung Lee and A Khitrin. Stimulated wave of polarization in a one-dimensional ising chain. *Physical Review A*, 71(6):062338, Jun 2005.

[11] Carlos A Perez-Delgado, Michele Mosca, Paola Cappellaro, and David G Cory. Single spin measurement using cellular automata techniques. *Physical review letters*, 97(10):100501, Jan 2006.

[12] RP STANLEY. Fibonacci lattice. *Fibonacci Quart*, 13(3):215–232, Jan 1975.

[13] B Sagan. The symmetric group: representations, combinatorial algorithms, and symmetric functions. *Springer*, pages 191–197, Jan 2001.

[14] J Fitzsimons and J Twamley. Superballistic diffusion of entanglement in disordered spin chains. *Physical Review A*, 72(5):050301, Jan 2005.

[15] E Farhi and S Gutmann. Quantum computation and decision trees. *Physical Review A*, 58(2):915–928, Jan 1998.

[16] C. H. Bennett and G. Brassard. Quantum cryptography: Public key distribution and coin tossing. *SIGACT News*, 15(78), 1983.

[17] Artur K. Ekert. Quantum cryptography based on bell's theorem. *Phys. Rev. Lett.*, 67:661–663, Aug 1991.

[18] E. Knill, R. Laflamme, and G. J. Milburn. A scheme for efficient quantum computation with linear optics. *Nature*, 409(6816):46–52, 2001.

[19] Pieter Kok, W. J. Munro, Kae Nemoto, T. C. Ralph, Jonathan P. Dowling, and G. J. Milburn. Linear optical quantum computing with photonic qubits. *Reviews of Modern Physics*, 79(2):797, 2007.

[20] P. Kok and B. W. Lovett. *Introduction to Optical Quantum Information Processing*. Cambridge University Press, 2010.

[21] Sean D. Barrett and Pieter Kok. Efficient high-fidelity quantum computation using matter qubits and linear optics. *Phys. Rev. A*, 71:060310, Jun 2005.

[22] S. Bose, P. L. Knight, M. B. Plenio, and V. Vedral. Proposal for teleportation of an atomic state via cavity decay. *Phys. Rev. Lett.*, 83:5158, 1999.

[23] Christoph Simon and William T. M. Irvine. Robust long-distance entanglement and a loophole-free bell test with ions and photons. *Phys. Rev. Lett.*, 91:110405, Sep 2003.

[24] Y. L. Lim, A. Beige, and L. C. Kwek. Repeat-until-success quantum computing. *Phys. Rev. Lett.*, 95:030505, 2005.

[25] R. Raussendorf and H. J. Briegel. A one-way quantum computer. *Phys. Rev. Lett.*, 86:5188, 2001.

[26] C. K. Hong, Z. Y. Ou, and L. Mandel. Measurement of subpicosecond time intervals between two photons by interference. *Phys. Rev. Lett.*, 59:2044–2046, Nov 1987.

[27] B. Lounis and M. Orrit. Single photon sources. *Rep. Prog. Phys.*, 68:1129, 2005.

[28] Axel Kuhn, Markus Hennrich, and Gerhard Rempe. Deterministic single-photon source for distributed quantum networking. *Phys. Rev. Lett.*, 89:067901, Jul 2002.

[29] J. McKeever, A. Boca, A. D. Boozer, R. Miller, J. R. Buck, A. Kuzmich, and H. J. Kimble. Deterministic generation of single photons from one atom trapped in a cavity. *Science*, 303(5666):1992–1994, 2004.

[30] B. Darquie, M. P. A. Jones, J. Dingjan, J. Beugnon, S. Bergamini, Y. Sortais, G. Messin, A. Browaeys, and P. Grangier. Controlled single-photon emission from a single trapped two-level atom. *Science*, 309(5733):454–456, 2005.

[31] Markus Hijlkema, Bernhard Weber, Holger P. Specht, Simon C. Webster, Axel Kuhn, and Gerhard Rempe. A single-photon server with just one atom. *Nat Phys*, 3(4):253–255, 2007.

[32] Satoshi Kako, Charles Santori, Katsuyuki Hoshino, Stephan Gotzinger, Yoshihisa Yamamoto, and Yasuhiko Arakawa. A gallium nitride single-photon source operating at 200 k. *Nat Mater*, 5(11):887–892, 2006.

[33] K. Hennessy, A. Badolato, M. Winger, D. Gerace, M. Atature, S. Gulde, S. Falt, E. L. Hu, and A. Imamoglu. Quantum nature of a strongly coupled single quantum dot-cavity system. *Nature*, 445(7130):896–899, 2007.

[34] E. Wu, J. R. Rabeau, G. Roger, F. Treussart, H. Zeng, P. Grangier, S. Prawer, and J.-F. Roch. Room temperature triggered single-photon source in the near infrared. *New Journal of Physics*, 9(12):434, 2007.

[35] Hannes Bernien, Lilian Childress, Lucio Robledo, Matthew Markham, Daniel Twitchen, and Ronald Hanson. Two-photon quantum interference from separate nitrogen vacancy centers in diamond. *Phys. Rev. Lett.*, 108:043604, Jan 2012.

[36] A. Sipahigil, M. L. Goldman, E. Togan, Y. Chu, M. Markham, D. J. Twitchen, A. S. Zibrov, A. Kubanek, and M. D. Lukin. Quantum interference of single photons from remote nitrogen-vacancy centers in diamond. *Phys. Rev. Lett.*, 108:143601, Apr 2012.

[37] Edward B. Flagg, Andreas Muller, Sergey V. Polyakov, Alex Ling, Alan Migdall, and Glenn S. Solomon. Interference of single photons from two separate semiconductor quantum dots. *Phys. Rev. Lett.*, 104:137401, Apr 2010.

[38] Raj B. Patel, Anthony J. Bennett, Ian Farrer, Christine A. Nicoll, David A. Ritchie, and Andrew J. Shields. Two-photon interference of the emission from electrically tunable remote quantum dots. *Nat Photon*, 4(9):632–635, 09 2010.

[39] Chun-Hsu Su, Andrew D. Greentree, and Lloyd C. L. Hollenberg. Towards a picosecond transform-limited nitrogen-vacancy based single photon source. *Opt. Express*, 16(9):6240–6250, Apr 2008.

[40] A. Kiraz, M. Atatüre, and A. Imamoğlu. Quantum-dot single-photon sources: Prospects for applications in linear optics quantum-information processing. *Phys. Rev. A*, 69:032305, Mar 2004.

[41] Charles Santori, David Fattal, Kai-Mei C Fu, Paul E Barclay, and Raymond G Beausoleil. On the indistinguishability of raman photons. *New Journal of Physics*, 11(12):123009, 2009.

[42] A. Nazir and S. D. Barrett. Overcoming non-markovian dephasing in single-photon sources through postselection. *Phys. Rev. A*, 79:011804, Jan 2009.

[43] E. M. Purcell. Long lived coherence in self-assembled quantum dots. *Physical Review*, 69:681, 1946.

[44] Dirk Englund, David Fattal, Edo Waks, Glenn Solomon, Bingyang Zhang, Toshihiro Nakaoka, Yasuhiko Arakawa, Yoshihisa Yamamoto, and Jelena Vučković. Controlling the spontaneous emission rate of single quantum dots in a two-dimensional photonic crystal. *Phys. Rev. Lett.*, 95:013904, Jul 2005.

[45] A. Auffèves, D. Gerace, J.-M. Gérard, M. Fran ça Santos, L. C. Andreani, and J.-P. Poizat. Controlling the dynamics of a coupled atom-cavity system by pure dephasing. *Phys. Rev. B*, 81:245419, Jun 2010.

[46] A. J. Ramsay, Achanta Venu Gopal, E. M. Gauger, A. Nazir, B. W. Lovett, A. M. Fox, and M. S. Skolnick. Damping of exciton rabi rotations by acoustic phonons in optically excited InGaAs/GaAs quantum dots. *Phys. Rev. Lett.*, 104:017402, Jan 2010.

[47] Gerald D. Mahan. *Many Particle Physics (Physics of Solids and Liquids)*. Springer, 3rd edition, 2000.

[48] Erik M. Gauger, Simon C. Benjamin, Ahsan Nazir, and Brendon W. Lovett. High-fidelity all-optical control of quantum dot spins: Detailed study of the adiabatic approach. *Phys. Rev. B*, 77:115322, Mar 2008.

[49] Erik M Gauger and Joachim Wabnig. Heat pumping with optically driven excitons. *Physical Review B*, 82(7):1–4, 2010.

[50] H. P. Breuer and F. Petruccione. *The Theory of Open Quantum Systems*. Oxford University, 2002.

[51] A. J. Ramsay, T. Godden, S. J. Boyle, Erik M Gauger, Ahsan Nazir, Brendon W
Lovett, A. M. Fox, and M. S. Skolnick. Phonon-Induced Rabi-Frequency Renor-
malization of Optically Driven Single InGaAs/GaAs Quantum Dots. *Physical
Review Letters*, 105(17):177402, 2010.

[52] P. Kaer, P. Lodahl, A.-P. Jauho, and J. Mork. Microscopic the-
ory of indistinguishable single-photon emission from a quantum dot cou-
pled to a cavity: The role of non-markovian phonon-induced decoherence.
http://arxiv.org/abs/1203.6268, 2012.

[53] D.F. Walls and G.J. Milburn. *Quantum Optics*. Springer, 2 edition, 2008.

[54] L. Tian and H. J. Carmichael. Quantum trajectory simulations of two-state
behavior in an optical cavity containing one atom. *Phys. Rev. A*, 46:R6801–
R6804, Dec 1992.

[55] Arka Majumdar, Dirk Englund, Michal Bajcsy, and Jelena Vučković. Nonlinear
temporal dynamics of a strongly coupled quantum-dot˘cavity system. *Phys.
Rev. A*, 85(3):033802, Mar 2012.